POLARIZATION STRUCTURE OF CONOSCOPIC PATTERNS FOR PLANAR NEMATIC AND CHOLESTERIC LIQUID-CRYSTAL CELLS

R.G. VOVK, A.D. KISELEV

Institute of Physics, Nat. Acad. of Sci. of Ukraine
(46, Nauky Ave., Kyiv 03680, Ukraine; e-mail: roman.vovk@gmail.com)

PACS 42.25.Ja,78.90.+t

The distributions of light polarization in conoscopic patterns obtained for planar nematic and cholesteric liquid-crystal cells have been studied theoretically. The geometry of polarization patterns is characterized in terms of polarization singularities, such as C-points (points corresponding to circular polarization) and L-lines (lines corresponding to linear polarization of light). The conditions required for the formation of polarization singularities (C-point) in a conoscopic pattern ensemble parametrized by the polarization azimuth and the ellipticity of incidence light have been considered. The selectivity with respect to polarization parameters has been found to be a characteristic feature of those conditions.

1. Introduction

Interest in the polarization optics of anisotropic media has been considerably raised in recent years, which is particularly associated with a wide application of liquid crystal technologies [1, 2]. Liquid crystals (LCs) are anisotropic media, the anisotropy of which is governed by their orientational structure, the latter being sensitive to external fields and boundary conditions [3]. It is the optical properties of LCs that determine their technological importance.

Conoscopy has been successfully used for studying the orientational structure of LCs for a long time [4–6]. As is known, the essence of the conoscopic method consists in the study of LC specimens using diverging light beams in a system of crossed polarizers. As a result, a conoscopic pattern, which arises owing to the interference of four polarized characteristic modes of an LC cell, can be observed at the output of a conoscope. However, if a system of crossed polarizers is used, a substantial portion of information on the light polarization state is lost. At the same time, this information can be useful, e.g., when developing new and improving the existing methods of orientational structure identification in anisotropic media. Therefore, there emerges a problem of studying the polarization distributions of light, which the conoscopic patterns are based upon.

Such distributions can be referred to as polarization-resolved conoscopic patterns, whose geometric images are the field of polarization ellipses on the observation plane [7]. In our previous works [7, 8], the polarization singularities—C-points (the points, at which the polarization of light is circular) and L-lines (the lines, along which the light polarization is linear) – were used to characterize the geometry of polarization-resolved conoscopic patterns. It is the polarization singularities that are both stable topological defects [9] and important elements that characterize the geometry of non-uniformly polarized light fields [10, 11].

The most detailed analysis of the geometry of polarization-resolved conoscopic patterns was carried out in the case of homeotropically oriented nematic LCs [8], when an orientational structure is characterized by the cylindrical symmetry, with the rotation axis directed along a normal to the cell. In work [8], by changing the polarization parameters (the polarization azimuth and the incident wave ellipticity), we managed to study, both theoretically and experimentally, the behavior of C-points in the corresponding ensemble of polarization-resolved conoscopic patterns for a homeotropic nematic LC cell. The theoretical analysis also allowed us to obtain various scenarios for the creation and annihilation of C-points in such polarization distributions.

Certainly, the following step has to consist in studying the polarization-resolved conoscopic patterns of LCs with other orientational structures. Effects associ-

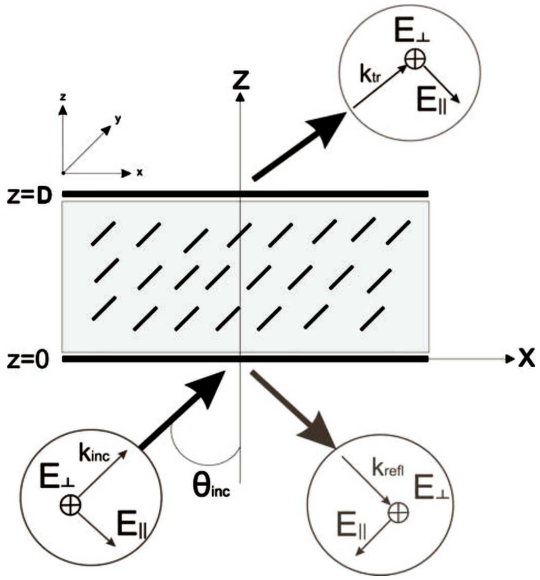

Fig. 1. Geometry of a nematic LC cell in the incidence plane

ated with a violation of the cylindrical symmetry of a homeotropic configuration should be expected to play the most important role. In order to study such effects in this work, we consider another limiting case where the optical axis of an anisotropic medium has a planar orientation. In particular, we will theoretically consider polarization-resolved conoscopic patterns given by planarly oriented nematic and cholesteric LC cells and determine conditions for the emergence of C-points in those polarization distributions.

2. Theory

Consider a nematic LC (NLC) cell with thickness D which is located between substrates, the normal to which is directed along the z-axis: $z = 0$ and $z = D$ (see Fig. 1). In the case of a planarly oriented nematic, the LC director $\hat{\mathbf{d}}$, which defines the orientation of the optical axis of NLC, lies in the substrate plane and is described by the expression

$$\hat{\mathbf{d}} = d_x\,\hat{\mathbf{x}} + d_y\,\hat{\mathbf{y}} = \cos\phi_{\rm d}\,\hat{\mathbf{x}} + \sin\phi_{\rm d}\,\hat{\mathbf{y}}, \tag{1}$$

where $\phi_{\rm d}$ is the azimuthal angle of the director. This angle is constant for a uniform planar NLC orientational structure, whereas the equilibrium configuration of the director in cholesteric LCs is described by Eq. (1) with the azimuthal angle $\phi_{\rm d} = qz + \phi_0$, where $q = 2\pi/P$ is the wave number of a cholesteric helix, and P is its step [3]. Certainly, if the step of a cholesteric helix tends to infinity, $\phi_{\rm d} = \phi_0$ in this case, and the planarly oriented nematic LC can be considered as a cholesteric one with an infinite step.

For the overwhelming majority of known nematics, their anisotropy is uniaxial, and the dielectric tensor of NLC has the general form [3]

$$\varepsilon = \varepsilon_\perp I_3 + \Delta\varepsilon\,\widehat{\mathbf{d}}\otimes\widehat{\mathbf{d}}, \tag{2}$$

where $\Delta\varepsilon = \varepsilon_\parallel - \varepsilon_\perp$, and I_n is the $n\times n$ identity matrix. The characteristic values of the tensor [3] correspond to the ordinary, $n_o = \sqrt{\mu\varepsilon_\perp}$, and extraordinary, $n_e = \sqrt{\mu\varepsilon_\parallel}$, refractive indices, where μ is the magnetic permeability of NLC.

We admit below that the environment is isotropic, with the dielectric constant ϵ_m and the magnetic permeability μ_m. Figure 1 demonstrates that there are two plane waves in the half-space $z \le 0$, namely, an incident wave $\{\mathbf{E}_{\rm inc}, \mathbf{H}_{\rm inc}\}$ and the reflected one $\{\mathbf{E}_{\rm refl}, \mathbf{H}_{\rm refl}\}$. The transmitted wave $\{\mathbf{E}_{\rm tr}, \mathbf{H}_{\rm tr}\}$ and the reflected one are excited by the incident wave, and they propagate in parallel in the half-space $z \ge D$. Hence, the field outside the cell is

$$\mathbf{E}|_{z<0} = \mathbf{E}_{\rm inc}(\hat{\mathbf{k}}_{\rm inc})e^{i(\mathbf{k}_{\rm inc}\cdot\mathbf{r})} + \mathbf{E}_{\rm refl}(\hat{\mathbf{k}}_{\rm refl})e^{i(\mathbf{k}_{\rm refl}\cdot\mathbf{r})}, \tag{3a}$$

$$\mathbf{E}|_{z>D} = \mathbf{E}_{\rm tr}(\hat{\mathbf{k}}_{\rm tr})e^{i(\mathbf{k}_{\rm tr}\cdot\mathbf{r})}, \tag{3b}$$

where, as a result of boundary conditions – the continuity of tangential components of electric and magnetic fields – the wave vectors $\mathbf{k}_{\rm inc}$, $\mathbf{k}_{\rm refl}$, and $\mathbf{k}_{\rm tr}$ lie in the plane of incidence (the $x-z$ coordinate plane) and look like

$$\mathbf{k}_\alpha = k_{\rm vac}\mathbf{q}_\alpha = k_{\rm m}\hat{\mathbf{k}}_\alpha = k_x\,\hat{\mathbf{x}} + k_z^{(\alpha)}\,\hat{\mathbf{z}}, \tag{4}$$

$\alpha \in \{\text{inc}, \text{refl}, \text{tr}\}$, $k_{\rm m}/k_{\rm vac} = n_{\rm m} = \sqrt{\mu_{\rm m}\epsilon_{\rm m}}$ is the refractive index of the environment, and $k_{\rm vac} = \omega/c = 2\pi/\lambda$ is the wave number in vacuum. The components of wave vectors are expressed in terms of the incidence angle $\theta_{\rm inc}$ as follows:

$$k_x = k_{\rm m}\sin\theta_{\rm inc} \equiv k_{\rm vac}\,q_x, \tag{5}$$

$$k_z^{(\rm inc)} = k_z^{(\rm tr)} = -k_z^{(\rm refl)} = k_{\rm m}\cos\theta_{\rm inc} \equiv k_{\rm vac}\,q_{\rm m}, \tag{6}$$

$$q_x = n_{\rm m}\sin\theta_{\rm inc}, \quad q_{\rm m} = \sqrt{n_{\rm m}^2 - q_x^2}. \tag{7}$$

The vector amplitudes of the electric fields of plane waves are

$$\mathbf{E}_\alpha(\hat{\mathbf{k}}_\alpha) = E_\parallel^{(\alpha)}\big(k_z^{(\alpha)}\,\hat{\mathbf{x}} - k_x\,\hat{\mathbf{z}}\big)k_{\rm m}^{-1} + E_\perp^{(\alpha)}\hat{\mathbf{y}}, \tag{8}$$

where $E_{\parallel}^{(\alpha)}$ and $E_{\perp}^{(\alpha)}$ are the electric field components that are oriented in parallel and perpendicularly, respectively, to the incidence plane.

The general form for electromagnetic fields of the incident, transmitted, and reflected waves propagating in the environment looks like

$$\{\mathbf{E},\mathbf{H}\} = \{\mathbf{E}(z),\mathbf{H}(z)\}\,\mathrm{e}^{i(k_x x-\omega t)}. \tag{9}$$

Using relations (9), it is also possible to obtain an equation for the tangential components of the electromagnetic field in an anisotropic layer. In the matrix form [12], it reads

$$-i\partial_\tau \mathbf{F} = \boldsymbol{\mathcal{M}}\cdot\mathbf{F} \equiv \begin{pmatrix} \boldsymbol{\mathcal{M}}_{11} & \boldsymbol{\mathcal{M}}_{12} \\ \boldsymbol{\mathcal{M}}_{21} & \boldsymbol{\mathcal{M}}_{22} \end{pmatrix} \begin{pmatrix} \mathbf{E}_P \\ \mathbf{H}_P \end{pmatrix}, \quad \tau \equiv k_{\mathrm{vac}} z, \tag{10}$$

where $\mathbf{E}_P = (E_x, E_y)^T$ and $\mathbf{H}_P = (H_y, -H_x)^T$.

General expressions for the 2×2 matrices $\boldsymbol{\mathcal{M}}_{ij}$, which characterize the block structure of the matrix $\boldsymbol{\mathcal{M}}$, are presented in works [7, 8]. For dielectric tensor (2) and director (1), the matrices $\boldsymbol{\mathcal{M}}_{ij}$ look like

$$\boldsymbol{\mathcal{M}}_{12} = \mu\boldsymbol{\mathcal{I}}_2 - \frac{q_x^2}{\epsilon_\perp}\,\mathrm{diag}(1,0), \quad \boldsymbol{\mathcal{M}}_{ii} = 0, \tag{11}$$

$$\boldsymbol{\mathcal{M}}_{21} = -\frac{q_x^2}{\mu}\,\mathrm{diag}(0,1) + \epsilon_c\boldsymbol{\mathcal{I}}_2 +$$

$$+\frac{\Delta\epsilon}{2}\begin{pmatrix} \cos(2\phi_\mathrm{d}) & \sin(2\phi_\mathrm{d}) \\ \sin(2\phi_\mathrm{d}) & -\cos(2\phi_\mathrm{d}) \end{pmatrix}, \tag{12}$$

where $\epsilon_c = (\epsilon_\parallel + \epsilon_\perp)/2$.

As a solution of the boundary-value problem, we obtain linear relations between the components of incident, transmitted, and reflected waves:

$$\begin{pmatrix} E_\parallel^{(\mathrm{tr})} \\ E_\perp^{(\mathrm{tr})} \end{pmatrix} = \boldsymbol{\mathcal{T}} \begin{pmatrix} E_\parallel^{(\mathrm{inc})} \\ E_\perp^{(\mathrm{inc})} \end{pmatrix}, \begin{pmatrix} E_\parallel^{(\mathrm{refl})} \\ E_\perp^{(\mathrm{refl})} \end{pmatrix} = \boldsymbol{\mathcal{R}} \begin{pmatrix} E_\parallel^{(\mathrm{inc})} \\ E_\perp^{(\mathrm{inc})} \end{pmatrix}, \tag{13}$$

where $\boldsymbol{\mathcal{T}}$ and $\boldsymbol{\mathcal{R}}$ are the transmission and reflection matrices, respectively. The main problem consists in calculating those two matrices.

In works [7, 8], it was shown that, in order to find the matrices $\boldsymbol{\mathcal{T}}$ and $\boldsymbol{\mathcal{R}}$, it is necessary to calculate the matrix

$$\boldsymbol{\mathcal{W}} = \boldsymbol{\mathcal{V}}_\mathrm{m}^{-1}\cdot\boldsymbol{\mathcal{U}}^{-1}\cdot\boldsymbol{\mathcal{V}}_\mathrm{m} = \begin{pmatrix} \boldsymbol{\mathcal{W}}_{11} & \boldsymbol{\mathcal{W}}_{12} \\ \boldsymbol{\mathcal{W}}_{21} & \boldsymbol{\mathcal{W}}_{22} \end{pmatrix} \tag{14}$$

and take advantage of the relations

$$\boldsymbol{\mathcal{T}} = \boldsymbol{\mathcal{W}}_{11}^{-1}, \tag{15}$$

$$\boldsymbol{\mathcal{R}} = \boldsymbol{\mathcal{W}}_{21}\cdot\boldsymbol{\mathcal{W}}_{11}^{-1} = \boldsymbol{\mathcal{W}}_{21}\cdot\boldsymbol{\mathcal{T}} \tag{16}$$

which connect the transmission and reflection matrices with the block matrices $\boldsymbol{\mathcal{W}}_{11}$ and $\boldsymbol{\mathcal{W}}_{21}$.

The expression for matrix (14) includes the inverse evolution operator $\boldsymbol{\mathcal{U}}^{-1} = \boldsymbol{\mathcal{U}}^{-1}(h,0) = \boldsymbol{\mathcal{U}}(0,h)$, where $h = k_{\mathrm{vac}}D$, and the operator $\boldsymbol{\mathcal{U}}(\tau,\tau_0)$ is a solution of the Cauchy matrix problem

$$-i\partial_\tau\boldsymbol{\mathcal{U}}(\tau,\tau_0) = \boldsymbol{\mathcal{M}}\cdot\boldsymbol{\mathcal{U}}(\tau,\tau_0), \quad \boldsymbol{\mathcal{U}}(\tau_0,\tau_0) = \boldsymbol{\mathcal{I}}_4, \tag{17}$$

as well as the matrix of characteristic vectors for the environment,

$$\boldsymbol{\mathcal{V}}_\mathrm{m} = \begin{pmatrix} \boldsymbol{\mathcal{E}}_\mathrm{m} & -\boldsymbol{\sigma}_3\boldsymbol{\mathcal{E}}_\mathrm{m} \\ \boldsymbol{\mathcal{H}}_\mathrm{m} & \boldsymbol{\sigma}_3\boldsymbol{\mathcal{H}}_\mathrm{m} \end{pmatrix} \tag{18}$$

characterized by two diagonal 2×2 matrices $\boldsymbol{\mathcal{E}}_\mathrm{m} = \mathrm{diag}(q_\mathrm{m}/n_\mathrm{m}, 1)$ and $\mu_\mathrm{m}\,\boldsymbol{\mathcal{H}}_\mathrm{m} = \mathrm{diag}(n_\mathrm{m}, q_\mathrm{m})$, where $\boldsymbol{\sigma}_3 = \mathrm{diag}(1,-1)$.

It is known that analytical expressions for the evolution operator and the transmission matrix of a cholesteric LC can be obtained only in the case of normal light incidence on an LC cell, when $q_x = 0$. In the case of the oblique incidence with $q_x \neq 0$, the system of equations (17) can be solved only numerically. Therefore, we present analytical results only for the transmission matrix of a nematic LC.

For the characteristic waves of an electromagnetic field in NLC, let us determine a matrix composed of characteristic values,

$$\boldsymbol{\mathcal{Q}} = \mathrm{diag}(q_e, q_o), \tag{19}$$

$$q_e = \sqrt{n_e^2 - q_x^2(1+u_a d_x^2)}, \quad q_o = \sqrt{n_o^2 - q_x^2}, \tag{20}$$

where $u_a = \Delta\epsilon/\epsilon_\perp$ is the anisotropy parameter of an NLC specimen, and two block matrices of characteristic vectors are

$$\boldsymbol{\mathcal{E}} = \mu\begin{pmatrix} d_x[1-q_x^2/n_o^2] & d_y q_o \\ d_y & -d_x q_o \end{pmatrix}, \tag{21}$$

$$\boldsymbol{\mathcal{H}} = \begin{pmatrix} d_x q_e & d_y n_o^2 \\ d_y q_e & -d_x[n_o^2 - q_x^2] \end{pmatrix}. \tag{22}$$

Then, we have the following expression for matrix (14):

$$\boldsymbol{\mathcal{W}} = N_\mathrm{m}^{-1}\,\mathrm{diag}(\boldsymbol{\mathcal{I}}_2, \boldsymbol{\sigma}_3)\cdot\tilde{\boldsymbol{\mathcal{W}}}\cdot\mathrm{diag}(\boldsymbol{\mathcal{I}}_2, \boldsymbol{\sigma}_3), \tag{23}$$

$$\tilde{\boldsymbol{\mathcal{W}}} = \begin{pmatrix} \boldsymbol{\mathcal{A}}_+ & \boldsymbol{\mathcal{A}}_- \\ \boldsymbol{\mathcal{A}}_- & \boldsymbol{\mathcal{A}}_+ \end{pmatrix} \cdot \boldsymbol{\mathcal{W}}_{\rm d} \cdot \begin{pmatrix} \boldsymbol{\mathcal{A}}_+^T & -\boldsymbol{\mathcal{A}}_-^T \\ -\boldsymbol{\mathcal{A}}_-^T & \boldsymbol{\mathcal{A}}_+^T \end{pmatrix}, \tag{24}$$

$$\boldsymbol{\mathcal{W}}_{\rm d} = \begin{pmatrix} \boldsymbol{\mathcal{W}}_- & \mathbf{0} \\ \mathbf{0} & \boldsymbol{\mathcal{W}}_+ \end{pmatrix}, \quad \boldsymbol{\mathcal{W}}_\pm = \exp[\pm i\boldsymbol{\mathcal{Q}}h] \cdot \boldsymbol{\mathcal{N}}^{-1}, \tag{25}$$

$$\boldsymbol{\mathcal{A}}_\pm = \boldsymbol{\mathcal{E}}_{\rm m} \cdot \boldsymbol{\mathcal{H}} \pm \boldsymbol{\mathcal{H}}_{\rm m} \cdot \boldsymbol{\mathcal{E}}, \quad \boldsymbol{\mathcal{N}} = {\rm diag}(N_e, N_o), \tag{26}$$

$$N_e = \frac{2q_e\mu}{n_o^2}(n_o^2 - q_x^2 d_x^2), \quad N_o = 2q_o\mu(n_o^2 - q_x^2 d_x^2), \tag{27}$$

where $N_{\rm m} = 2q_{\rm m}/\mu_{\rm m}$.

We substitute Eqs. (23)–(27) into relations (15) and (16) to obtain the following expressions for the transmission and reflection matrices:

$$\boldsymbol{\mathcal{T}} = N_{\rm m}\tilde{\boldsymbol{\mathcal{W}}}_{11}^{-1}, \quad \boldsymbol{\mathcal{R}} = \boldsymbol{\sigma}_3 \cdot \tilde{\boldsymbol{\mathcal{W}}}_{21} \cdot \tilde{\boldsymbol{\mathcal{W}}}_{11}^{-1}, \tag{28}$$

$$\tilde{\boldsymbol{\mathcal{W}}}_{11} = \boldsymbol{\mathcal{A}}_+ \cdot \boldsymbol{\mathcal{W}}_- \cdot \boldsymbol{\mathcal{A}}_+^T - \boldsymbol{\mathcal{A}}_- \cdot \boldsymbol{\mathcal{W}}_+ \cdot \boldsymbol{\mathcal{A}}_-^T, \tag{29}$$

$$\tilde{\boldsymbol{\mathcal{W}}}_{21} = \boldsymbol{\mathcal{A}}_- \cdot \boldsymbol{\mathcal{W}}_- \cdot \boldsymbol{\mathcal{A}}_+^T - \boldsymbol{\mathcal{A}}_+ \cdot \boldsymbol{\mathcal{W}}_+ \cdot \boldsymbol{\mathcal{A}}_-^T. \tag{30}$$

It should be noted that the transmission matrix $\boldsymbol{\mathcal{T}}$ is calculated in the incidence plane. It determines the transmission matrix of conoscopic patterns, $\tilde{\boldsymbol{\mathcal{T}}}$, which is described in the circular basis by the relation [7, 8]

$$\tilde{\boldsymbol{\mathcal{T}}}(\rho, \phi) = \exp(-i\phi\,\boldsymbol{\sigma}_3)\boldsymbol{\mathcal{T}}_c(\rho, \phi_{\rm d} - \phi)\exp(i\phi\,\boldsymbol{\sigma}_3), \tag{31}$$

$$\rho = r\tan\theta_{\rm inc}, \quad \phi = \phi_{\rm inc}, \tag{32}$$

where $\boldsymbol{\mathcal{T}}_c = \boldsymbol{\mathcal{C}}\boldsymbol{\mathcal{T}}\boldsymbol{\mathcal{C}}^\dagger$, $\boldsymbol{\mathcal{C}} = 2^{-1/2}\begin{pmatrix} 1 & -i \\ 1 & i \end{pmatrix}$, and r is the aperture-dependent scale factor. In the plane of conoscopic pattern observation, ρ and ϕ are the polar coordinates (the Cartesian coordinates are $x = \rho\cos\phi$ and $y = \rho\sin\phi$), which are determined by the incidence angle $\theta_{\rm inc}$ and the azimuthal angle of the incidence plane $\phi_{\rm inc}$.

It is important to note that the transmission matrix (31) does not depend on the azimuthal angle of the incidence plane ϕ at the center of the conoscopic pattern ($\rho = 0$), which corresponds to the case of normal incidence ($\theta_{\rm inc} = 0$). Using the analytical results for transmission matrices of NLC and CLC cells at $q_x = 0$, one can demonstrate that

$$\tilde{\boldsymbol{\mathcal{T}}}\Big|_{\rho=0} = \boldsymbol{\mathcal{T}}_c(0, \phi_{\rm d}). \tag{33}$$

3. Polarization-resolved Conoscopic Patterns

The transmission matrix (31) governs the distribution of circular components of a transmitted wave in the observation plane:

$$\begin{pmatrix} E_+^{\rm (tr)}(\rho,\phi) \\ E_-^{\rm (tr)}(\rho,\phi) \end{pmatrix} = \tilde{\boldsymbol{\mathcal{T}}}(\rho,\phi)\begin{pmatrix} E_+^{\rm (inc)} \\ E_-^{\rm (inc)} \end{pmatrix}, \tag{34}$$

where $E_\pm^{\rm (inc,\,tr)} = 2^{-1/2}\left(E_\parallel^{\rm (inc,\,tr)} \mp iE_\perp^{\rm (inc,\,tr)}\right)$. In particular, Eq. (34) allows one to calculate a polarization-resolved conoscopic pattern in the form of a polarization ellipse field. The latter is determined by the distribution of polarization parameters (the polarization azimuth $\phi_p^{\rm (tr)}$ and the ellipticity $\varepsilon_{\rm ell}^{\rm (tr)}$) of a transmitted wave in the plane of observation. Those parameters can be easily found from the equations

$$2\phi_p = \arg(E_+^* E_-) = \arctan\left[\frac{S_2}{S_1}\right], \tag{35}$$

$$\varepsilon_{\rm ell} = \frac{|E_+| - |E_-|}{|E_+| + |E_-|} = \tan\left[\frac{1}{2}\arcsin\left(\frac{S_3}{S_0}\right)\right], \tag{36}$$

where $E_\pm = |E_\pm|\exp(i\phi_\pm)$; and S_0, S_1, S_2, and S_3 are the Stokes parameters [13], for which the relations

$$S_0 = |E_+|^2 + |E_-|^2 = \sqrt{S_1^2 + S_2^2 + S_3^2}, \tag{37a}$$

$$S_1 = 2\,{\rm Re}(E_+^* E_-) = S_0\cos 2\chi_p \cos 2\phi_p, \tag{37b}$$

$$S_2 = 2\,{\rm Im}(E_+^* E_-) = S_0\cos 2\chi_p \sin 2\phi_p, \tag{37c}$$

$$S_3 = |E_+|^2 - |E_-|^2 = S_0\sin 2\chi_p \tag{37d}$$

define a Poincaré sphere parametrized by means of the polarization azimuth, $0 < \phi_p \le \pi$, and the ellipticity angle, $-\pi/4 \le \chi_p \le \pi/4$. At $E_\pm = E_\pm^{\rm (inc)}$ ($E_\pm = E_\pm^{\rm (tr)}$), Eqs. (35) and (36) give the polarization azimuth $\phi_p^{\rm (inc)}$ ($\phi_p^{\rm (tr)}$) and the ellipticity $\varepsilon_{\rm ell}^{\rm (inc)}$ ($\varepsilon_{\rm ell}^{\rm (tr)}$) of an incident (transmitted) wave.

If $|E_\nu| = 0$, the wave is circularly polarized, and its phase ϕ_ν together with the polarization azimuth ϕ_p is uncertain. Therefore, such a polarization singularity can be regarded as a phase singularity of the Stokes complex field $S = S_1 + iS_2 = E_+^* E_-$. The points with $|E_\nu| = 0$, where $\varepsilon_{\rm ell} = -\nu$, will be referred to as C-points.

In the linear polarization case, $|E_+| = |E_-|$, and the polarization sign is uncertain. The curves of linear polarization will be referred as L-lines. In the case of random non-uniformly polarized light fields, L-lines divide the regions with left and right polarizations [10].

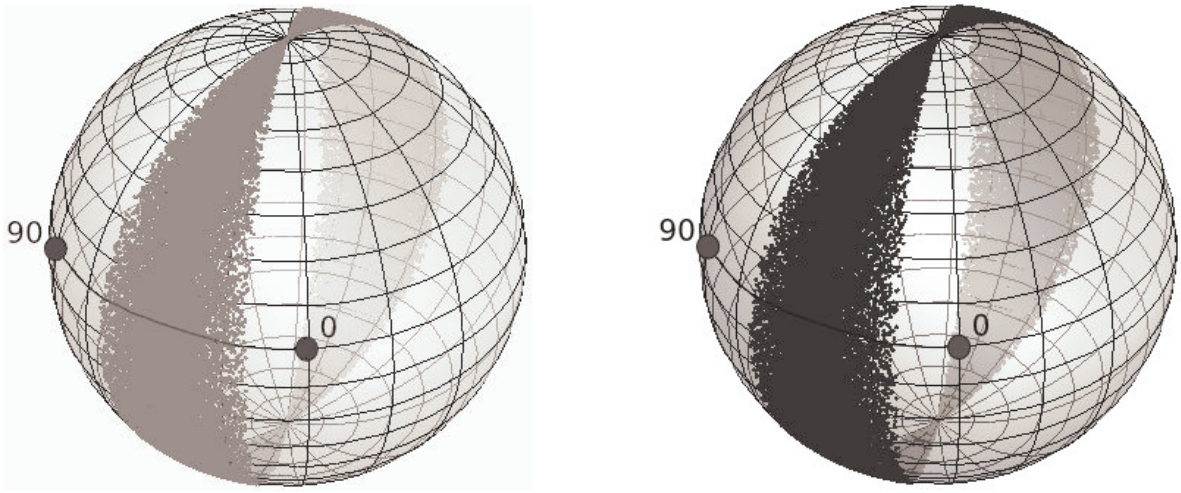

a **b**

Fig. 2. Polarization states that induce left (*a*) and right (*b*) *C*-points in polarization-resolved conoscopic patterns of a planarly oriented nematic. The calculation parameters: nematic LC E7 ($n_o = 1.54$, $n_e = 1.72$), $n_m = 1.5$, the cell thickness $D = 100$ μm, the light beam aperture is 30°, and $\phi_{\rm d} = 0$. The directions of variations of the polarization azimuth and its values are shown on the spheres

3.1. Planar orientation

Consider the conditions needed for C_ν-points to emerge in the polarization-resolved conoscopic patterns of a planar NLC cell. Since the transmission matrix $\tilde{\boldsymbol{\mathcal{T}}}(\rho, \phi)$ depends on two angles of light-wave incidence onto the cell, we may admit that only light waves with a certain polarization state can induce C_ν-points. To find such states of light wave polarization, let us solve the inverse problem of light transmission. Knowing the polarization state of light at the C_ν-point and the transmission matrix for a cell, it is possible to obtain the polarization state of an incident light wave that induces the polarization singularity. For this purpose, let us substitute the vector of circular components of the transmitted wave – it looks like $(1, 0)^T$ for a right C-point and $(0, 1)^T$ for a left one – into Eq. (34). By varying the incidence angles $\theta_{\rm inc}$ and $\phi_{\rm inc}$ (or ρ and ϕ), we obtain the polarization states for the incident wave which induce C_ν-points. The latter will be represented by points on the Poincaré sphere.

In Fig. 2, the regions of incident-wave polarization states are presented on the Poincaré sphere (parallels correspond to the polarization azimuth, and meridians to the ellipticity), at which the polarization-resolved conoscopic pattern contains at least one C_ν-point. The corresponding calculation parameters are given in the figure caption. From this figure, one can see that, in contrast to a homeotropically oriented NLC, for which the relevant region covers the whole Poincaré sphere, in the case of planar director orientation, there is a substantial dependence of the C-point formation conditions on the azimuthal angle of the incident wave polarization $\phi_p^{(\rm inc)}$. The Poincaré spheres depicted in Fig. 2 were calculated for the case $\phi_{\rm d} = 0$. The change of the angle $\phi_{\rm d}$ is accompanied by the motion of the regions along parallels.

The previous conclusion is also confirmed by the angular polarization distributions for a planarly oriented NLC which are shown in Fig. 3. In particular, in the polarization-resolved conoscopic pattern depicted in Fig. 3,*b*, there are C-points which form a regular geometric structure. It is also worth noting that, similarly to what takes place in the polarization-resolved conoscopic patterns of a homeotropically oriented nematic LC, there exist the effects of structural instability of the intersection between L-lines and the sign alternation for the topological index of C-points [8].

3.2. Cholesteric helix

It is interesting to study what happens to the regions that induce C-points (Fig. 2), when a chirality appears in the CLC cell, so that a helical structure of the director emerges with a non-zero wave number of the CLC helix, $q \neq 0$, and a finite corresponding value of the helix step, $P = 2\pi/q$. Since a planarly oriented nematic LC can be considered as a cholesteric one with the infinite step, we fix below, for convenience, the cholesteric helix step as a multiple of the LC cell thickness D.

In Fig. 4, we present the regions on the Poincaré sphere which induce C-points in polarization-resolved conoscopic patterns of a cholesteric LC. In the first case (Fig. 4,*a*), the situation where certain polarization states

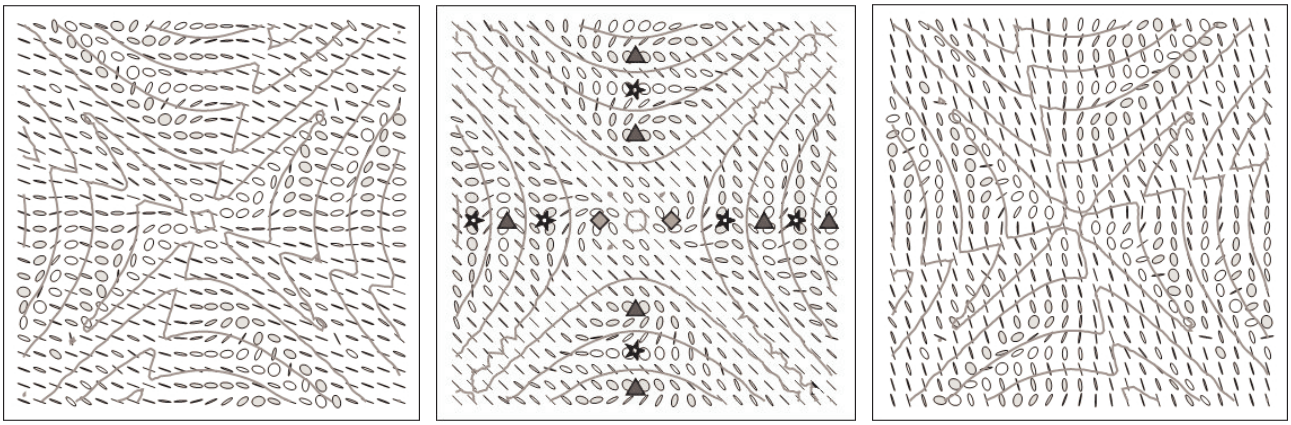

a **b** **c**

Fig. 3. Polarization-resolved conoscopic patterns of a planarly oriented NLC cell obtained for a linearly polarized incident wave with $\phi_p^{\rm inc} = 20$ (a), 45 (b), and 75° (c). The calculation parameters are the same as in Fig. 2. C-points of the *star*, *monstar*, and *lemon* types [10] are designated by stars, triangles, and rhombs, respectively. L-lines are designated by dark curves. Light and dark ellipses correspond to right and left polarizations, respectively

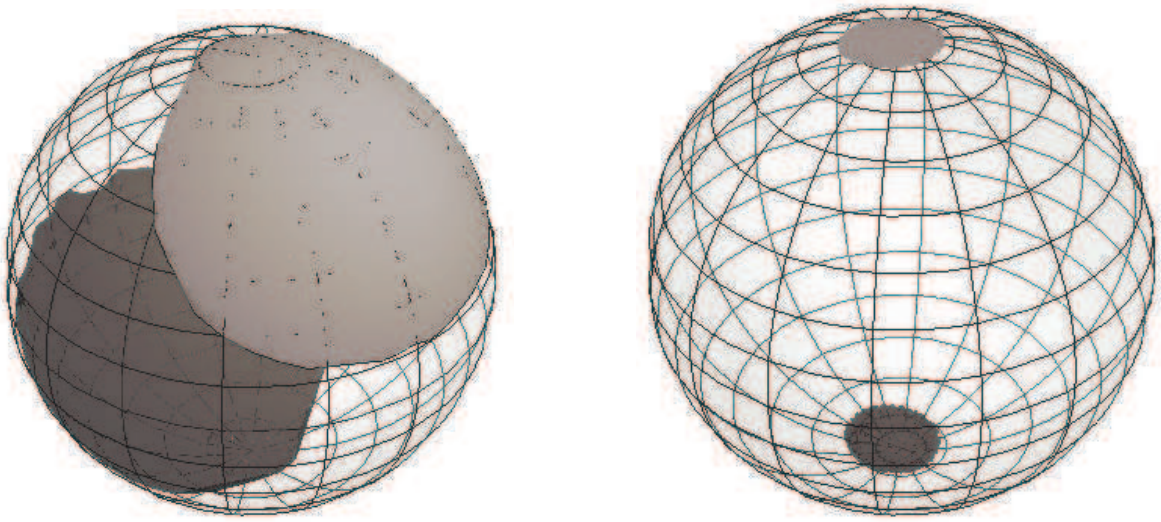

a **b**

Fig. 4. Polarization states of an incident light wave that induce C-points in polarization-resolved conoscopic patterns of a cholesteric LC. The calculation parameters: nematic LC E7 with a chiral additive ($n_o = 1.54$, $n_e = 1.72$), $n_m = 1.5$, the cell thickness $D = 100$ μm, the light beam aperture is 30°, the cholesteric helix step $P = 250$ (a) and 200 μm (b). The regions that induce right (left) C-points are marked as grey (dark grey)

induce either right or left C-points only arises already when the cholesteric helix step $P = 250$ μm. As it was for NLCs cells, the dependence on the azimuthal angle $\phi_p^{\rm (inc)}$ still remains in this case, but, additionally, there emerges a dependence on the incident wave ellipticity $\varepsilon_{\rm ell}^{\rm (inc)}$.

If the cholesteric helix step diminishes to $P = 200$ μm (Fig. 4,b), i.e. when a half-turn of the helix is formed, the regions that induce C-points move toward the sphere poles. Provided that two half-turns of the helix are formed in the cell, i.e. at $P = 100$ μm, those regions transform into two separate bands on the Poincaré sphere (see Fig. 5,a).

One can see that, in those cases where an integer number of cholesteric helix half-turns is formed in the cell, the corresponding regions on the Poincaré sphere of an incident wave become cylindrically symmetric, and, hence, the dependence of the conditions of C-point emer-

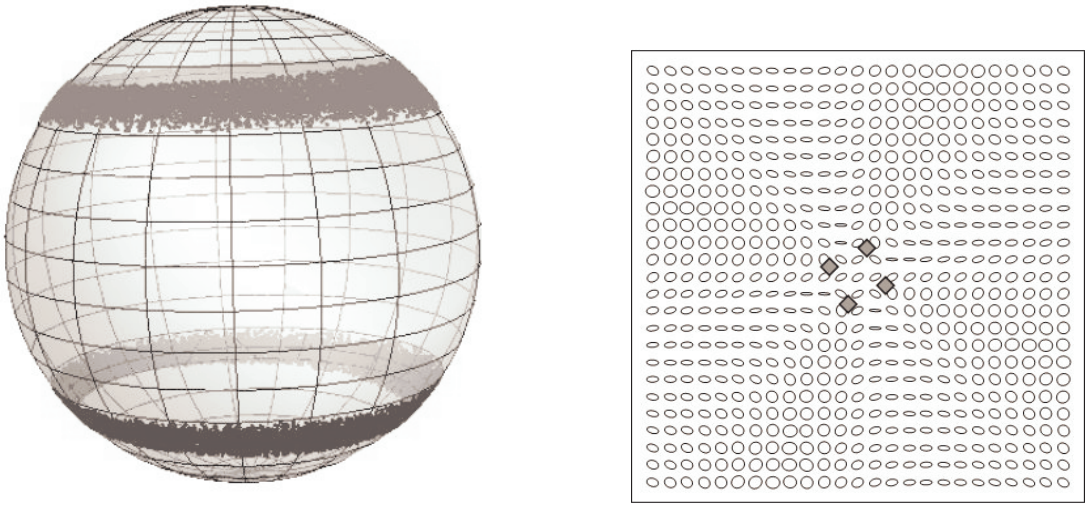

a **b**

Fig. 5. (*a*) Polarization states of an incident light wave that induce C-points and (*b*) a typical polarization-resolved conoscopic pattern for a cholesteric LC ($\varepsilon_{ell}^{\rm inc} = 0.7$, $\phi_p^{\rm inc} = 20°$). The calculation parameters: nematic LC E7 with a chiral additive ($n_o = 1.54$, $n_e = 1.72$), $n_m = 1.5$, the cell thickness $D = 100$ μm, the light beam aperture is 30°. The regions that induce right (left) C-points are marked as grey (dark grey). C-points of the *lemon* type are designated by rhombs

gence on the polarization azimuth $\phi_p^{\rm (inc)}$ disappears altogether. Therefore, the appearance of C-points in a polarization-resolved conoscopic pattern is completely governed by the value of incident-wave ellipticity $\varepsilon_{\rm ell}^{\rm (inc)}$.

For a cholesteric LC, the polarization-resolved conoscopic pattern looks like that presented in Fig. 5,*b*. It is evident that this pattern is composed of polarization ellipses of the same sign; i.e. C-points and L-lines exist separately in such polarization distributions.

4. Conclusions

A characteristic feature of polarization-resolved conoscopic patterns for planar nematic and cholesteric LC cells consists in the selectivity of C-point formation conditions with respect to the polarization parameters of incident light wave.

In the case of planarly oriented NLCs, it has been demonstrated that the appearance of C-points depends only on the polarization azimuthal angle $\phi_p^{\rm (inc)}$, whereas the incident wave ellipticity almost does not affect their formation. When the azimuthal angle of the director changes, the polarization state regions on the Poincaré sphere that induce C-points rotate around the S_3-axis. This testifies that the azimuthal angle selectivity is associated with a violation of the cylindrical symmetry in the homeotropic configuration.

In CLCs cells, the equilibrium configuration is a non-uniform helicoidal one, in which the director rotates around the normal to the cell. If the number of half-turns in the CLC helix is more than one, those rotations "restore" the cylindrical symmetry, so that the corresponding regions on the Poincaré sphere of an incident wave also become cylindrically symmetric. In this case, a crucial factor that governs the appearance of C-points is the incident wave ellipticity $\varepsilon_{\rm ell}^{\rm (inc)}$. Moreover, the regions of incident-wave polarization states that induce C-points with opposite chirality signs do not intersect. The indicated features can evidently be considered as effects of the CLC chirality.

To summarize, we note that a detailed analysis of transformations that the polarization-resolved conoscopic patterns of NLCs and CLC cells undergo at the variation of incident-wave polarization parameters testified to a universal character of bifurcation effects studied in work [8] for homeotropic structures. The results of those researches will be published elsewhere.

The work was partially supported financially by the Science and Technology Center in Ukraine (grant No. 4687).

1. P. Yeh and C. Gu, *Optics of Liquid Crystal Displays* (Wiley, New York, 1999).

2. V.G. Chigrinov, *Liquid Crystal Devices: Physics and Applications* (Artech House, Boston, 1999).

3. P.G. de Gennes and J. Prost, *The Physics of Liquid Crystals* (Clarendon Press, Oxford, 1993).

4. G. Baur, V. Wittwer, and D.W. Berreman, Phys. Lett. A **56**, 142 (1976).

5. L.H. Brett and H.H. Winter, Appl. Opt. **40**, 2089 (2001).

6. Yu.A. Nastishin, O.B. Dovgyi, and O.G. Vlokh, Ukr. J. Phys. Opt. **2**, N 2, 98 (2001).

7. A.D. Kiselev, J. Phys.: Condens. Matter, **19**, 246102 (2007).

8. A.D. Kiselev, R.G. Vovk, R.I. Egorov, and V.G. Chigrinov, Phys. Rev. A **78**, 033815 (2008).

9. N.D. Mermin, Rev. Mod. Phys. **51**, 591 (1979).

10. J.F. Nye, *Natural Focusing and Fine Structure of Light: Caustics and Wave Dislocations* (Institute of Physics, Bristol, 1999).

11. J.F. Nye, Proc. R. Soc. London, A **389**, 279 (1983).

12. D.W. Berreman, J. Opt. Soc. Am. **62**, 502 (1972).

13. M. Born and E.W. Wolf, *Principles of Optics* (Pergamon Press, Oxford, 1991).

Received 09.10.09.
Translated from Ukrainian by O.I. Voitenko

ПОЛЯРИЗАЦІЙНА СТРУКТУРА КОНОСКОПІЧНИХ КАРТИН ПЛАНАРНИХ НЕМАТИЧНИХ ТА ХОЛЕСТЕРИЧНИХ РІДКОКРИСТАЛІЧНИХ КОМІРОК

Р.Г. Вовк, О.Д. Киселъов

Р е з ю м е

Теоретично досліджено поляризаційні розподіли світла в коноскопічних картинах планарних нематичних та холестеричних рідкокристалічних комірок. Геометрію поляризаційних структур описано за допомогою поляризаційних сингулярностей: C-точок (точок з циркулярною поляризацією) і L-ліній (ліній, вздовж яких поляризація лінійна). Розглянуто умови формування поляризаційних сингулярностей (C-точок) в ансамблі коноскопічних картин, параметризованих азимутом поляризації і еліптичністю падаючої світлової хвилі. Показано, що характерною особливістю цих умов є селективність за поляризаційними параметрами.